

Special
Issue

Water-Assisted Chemical Route Towards the Oxygen Evolution Reaction at the Hydrated (110) Ruthenium Oxide Surface: Heterogeneous Catalysis via DFT-MD and Metadynamics Simulations

Fabrizio Creazzo^[a] and Sandra Luber^{*[a]}

Abstract: Notwithstanding that RuO₂ is a promising catalyst for the oxygen evolution reaction (OER), a plethora of fundamental details on its catalytic properties are still elusive, severely limiting its large-scale deployment. It is also established experimentally that corrosion and wettability of metal oxides can, in fact, enhance the catalytic activity for OER owing to the formation of a hydrated surface layer. However, the mechanistic interplay between surface wettability, interfacial water dynamics and OER across RuO₂, and what degree these processes are correlated are still debated. Herein, spin-polarized Density Functional Theory Molecular Dynamics (DFT-MD) simulations, coupled with advanced enhanced sampling methods in the well-tempered metadynamics framework, are applied to gain a global understanding of RuO₂ aqueous interface (explicit water solvent) in catalyzing the OER, and hence possibly help in the design of novel catalysts in the context of photochemical water oxidation.

The present study quantitatively assesses the free-energy barriers behind the OER at the (110)-RuO₂ catalyst surface revealing plausible pathways composing the reaction network of the O₂ evolution. In particular, OER is investigated at room temperature when such a surface is exposed to both gas-phase and liquid-phase water. Albeit a unique efficient pathway has been identified in the gas-phase OER, a surprisingly lowest-free-energy-requiring reaction route is possible when (110)-RuO₂ is in contact with explicit liquid water. By estimating the free-energy surfaces associated to these processes, we reveal a noticeable water-assisted OER mechanism which involves a crucial proton-transfer-step assisted by the local water environment. These findings pave the way toward the systematic usage of DFT-MD coupled with metadynamics techniques for the fine assessment of the activity of catalysts, considering finite-temperature and explicit-solvent effects.

Introduction


Solar power is by far the largest source of renewable energy ($\sim 1.2 \times 10^{14}$ kJ are received at the Earth's surface every second)^[1] and visible-light-driven water splitting is currently in the focus of worldwide research efforts toward clean and sustainable strategies which are facing the increasing demand for renewable energy.^[2,3] Nowadays, solar light-driven technology is undoubtedly a promising and reliable way to produce fuels from the water splitting reaction. Researchers in the field of artificial photosynthesis aim to achieve this by using sunlight to drive the production of so called solar fuels (e.g. H₂, MeOH) from the oxidation of water. Water oxidation, or Oxygen Evolution Reaction (OER) in a (photo)electrochemical cell, is

considered to be a major bottleneck and new catalysts capable to enhance this reaction are therefore constantly in high demand.^[4,5]

During the past decades, special emphasis has been placed on the development of efficient water oxidation catalysts (WOCs) to overcome the major roadblock in the way of solar hydrogen generation by photosynthesis. A prerequisite for smart design of more efficient WOCs is the understanding of the entire water oxidation process. The catalyst and its water oxidation behaviour have thus to be elucidated thoroughly. This includes the detailed structure of the catalyst as well as the mechanism of water oxidation and the related reaction networks. Generally, the complex process of photochemical water oxidation in WOC-photosensitizer systems is influenced by numerous parameters, and their individual impact on the WOC performance remains difficult to assess.^[6] In recent years, ruthenium-oxide-based catalysts have disclosed promising catalytic performance in a variety of important reactions such as the water oxidation.^[5,7] The efficiency of the WOC is mainly determined by the potential cost needed for the OER which is a thermodynamic up-hill reaction usually requiring a high potential to drive the reaction, and in this context ruthenium oxides have gained a lot of attention. First of all, ruthenium dioxide RuO₂ is a cheaper catalyst compared to costly platinum, iridium and titanium based-oxides, but with less^[8]/comparable^[9]

[a] Dr. F. Creazzo, Prof. S. Luber
Department of Chemistry,
University of Zurich,
Zurich, Switzerland
E-mail: sandra.luber@chem.uzh.ch

 Part of a Special Issue on Contemporary Challenges in Catalysis.

 © 2021 The Authors. Chemistry - A European Journal published by Wiley-VCH GmbH. This is an open access article under the terms of the Creative Commons Attribution Non-Commercial License, which permits use, distribution and reproduction in any medium, provided the original work is properly cited and is not used for commercial purposes.

OER electro-catalytic performance. Due to its high electronic conductivity (electrical resistivity is $35.2 \pm 0.5 \mu\Omega \times cm$ at room temperature), RuO₂,^[10] RuO₂ based/combined materials and Ru(O₂) ligands^[5] have turned out to be attractive oxidation catalysts in heterogeneous photo-catalysis and electro-catalysis and with a higher stability in the water oxidation potential region than costly catalysts.^[7] An additional advantage is that RuO₂ can be used as bi-catalyst (as anode and/or cathode), and hence it can be used for both water oxidation and Hydrogen Evolution Reaction (HER). It is not only the activity but rather its stability which renders RuO₂ an excellent material in operando conditions in the potential region of the HER.^[5,11,12] Furthermore, hydrated RuO₂ exhibits mixed electron-proton conductivity suitable for technological applications and opportunities in (photo)electrocatalysis and charge storage.^[7]

Despite the technological importance of RuO₂ this material has not been well characterized due to its structural disorder and variable chemistry, especially with respect to the oxidation state of Ru and its structural water or –OH content. To date, a wide range of studies shows the effect of rather diverse factors, such as crystal structure, morphology, composition, valence state, crystallinity, and even the buffer medium on water oxidation processes.^[5,7]

The lowest energy crystal planes of RuO₂ are (110), (100), and (101). From Density Functional Theory (DFT) static calculations, Over, Seitsonen and co-workers^[13] determined the surface energies of bulk-truncated RuO₂ (110), RuO₂ (100), and RuO₂ (101) to be 71 meV/Å², 87 meV/Å², and 76 meV/Å², respectively. Therefore the (110) orientation is expected to be the most abundant orientation of polycrystalline RuO₂ as highlighted by experimental studies.^[7,14–16] However, in the potential region of water splitting, the (100) and the (101) surfaces may also play a role.^[7] Note also the higher stability of the (111)-RuO₂ facet under catalytic conditions (high oxygen chemical potentials).^[17] However, most of the studies present in the literature are done only at the (110) RuO₂ facet because of the difficulties to mimic catalytic conditions as whole in DFT-MD simulations.^[18,19] Stamenkovic *et al.*^[20] and Rossmeisl *et al.*^[21] have studied the stability of the reaction intermediates for the OER over RuO₂-(110), using static DFT investigations for the thermochemistry of electrochemical reactions where the expected reactant water molecule is taken into account only implicitly (implicit solvent model, *i.e.* water is taken into account in the calculation of free-energy barriers). As shown in Ref. [21], only when the potential is above 1.6 V, all reaction steps are downhill in free energy, thus making OER feasible. A more recent theoretical study based on static DFT with implicit solvent model investigated the OER on RuO₂-(110) determining the reaction barriers involved in the elementary reaction steps.^[16] Above 1.58 V, the reaction occurred on the fully O-terminated phase. The rate determining step was identified with the water dissociation above the O-terminated RuO₂-(110) surface. Recently, DFT studies have shown how the inclusion and *in silico* design of ligands offer the possibility of fine-tuning the activity of the Ru metal core and a promising route for molecular catalysts.^[22–27] In addition, it was observed that

doping/mixing of RuO₂ with various elements, such as Ir, Co, Ce, Ni, Pb, and Zn, improves the water splitting activity.^[7]

The limits of most aforementioned theoretical surface-science calculations are the lack of finite temperature effects and explicit water environment which interacts with the surface catalyst and with the chemical compounds involved in the OER reaction. At the best, in general, only one water molecule/one water layer has been explicitly taken into account in the calculations of the OER at the RuO₂ as well as IrO₂,^[28–30] not enough to have a proper explicit water environment and to take into account its influence on the chemical OER pathway.

It is not only the explicit presence of the aqueous solvent that matters, *i.e.*, its structural organization at the interface with the catalyst, but the water dynamics at finite temperature also matters (e.g. wriggling of water at the surface, diffusion, dynamical charge transfers). The whole complex structure and dynamicity of the electric double layer (EDL) in the electro/photo chemical conditions have to be accounted for, as well as the presence of adsorbed species at the surface and at the interface for their influence on the EDL structure and hence on the chemical processes occurring at the aqueous interface. With this in mind, it is stating the obvious that catalytic reactions such as water oxidation/electrolysis/photolysis are highly complex to model because of the interplay in between the catalyst material (metal/semiconductor), the electrolyte in general, the liquid, the adsorbed species, or also the gas-phase vs liquid-phase reactants and products. Studies of bulk water, water solutions and water-air interface have shown the ability of a constant external electric field to induce a reorientation of water dipoles along the field direction, and hence enhancing the water dissociation.^[31–36] Although such a strategy nicely provides that the electric field can control the water dissociation, this is still not simulating photo-electrochemical conditions.

The design of catalysts cannot be done entirely from experiments, as it is complicated to individually tune the relevant microscopic parameters that enter into a catalyst and ascribe them directly to the cell performance. An atomistic probing and methods to tune one-by-one the parameters are required. None of these are obvious from experiments alone, while one would like to avoid costly ‘trial and error’ experiments. These represent a significant hurdle toward the development of improved catalysts, which could be overcome by employing methods able to track the catalytic features of the WOC at the atomistic scale. Atomistic simulations are a way to get this information. Disclosing the detailed mechanisms of water oxidation on ruthenium oxides surfaces – as well as the surface chemical reactivity and the involved reaction pathways – would have a crucial role in improving the efficiency of the catalyst and thus help for a better design.

Accordingly, the aim of the present research is to provide, via forefront DFT-MD and metadynamics simulations, a noticeable understanding of (110)-RuO₂-aqueous interface in catalyzing the OER in the context of solar light driven water splitting. By this way, we provide a full assessment of the kinetics and involved free-energy barriers behind the OER at the (110)-RuO₂

catalyst surface, helping thus in the design of RuO_2 as WOC in the context of structured (photo)electrochemical system.

Therefore, our research is focused on characterizing Ru-based photocatalysts to achieve efficient and long-term O_2 evolution from water under light irradiation. Explicit solvent model and its dynamics for the OER investigations provided in the present research could be the key for achieving considerable steps forward in the field.

The paper is organized as follow: the computational approach and (110)- RuO_2 model are highlighted in Section *Computational methods*; Section *Modelling the OER at the (110)- RuO_2* focus on how to properly model the OER in gas-phase and in explicit solvent model, whereas Section *OER activity descriptors* highlights the OER activity descriptor adopted in our investigation; Section *OER at the hydrated (110)- RuO_2 facet: gas-phase solvent model* and Section *OER at the hydrated (110)- RuO_2 facet: liquid-phase solvent model* finally show and compare our OER metadynamics results in gas-phase and liquid-phase, respectively, revealing a noticeable water-assisted OER chemical pathway. Further calculations about oxidation state during OER are also outlined in Section *OER at the hydrated (110)- RuO_2 facet: liquid-phase solvent model*. Finally, in Section *Conclusions* we summarize the main conclusions of our work.

Computational methods

Spin-polarized Kohn-Sham DFT-MD has been performed in the Born-Oppenheimer framework employing the CP2K program package.^[37,38] The PBE^[39] exchange-correlation functional, shown to be reliable for the description of properties of ruthenium oxide and liquid water,^[40–43] has been adopted as well as GTH pseudopotentials.^[44]

The DZVP-MOLOPT-SR basis set^[45] and a 400 Ry plane wave basis set have been used, being a good compromise between computational cost and accuracy. Grimme's D2 dispersion correction^[46,47] has been adopted. Periodic boundary conditions (PBCs) have been applied in all three spatial directions. The spin-polarized DFT-MD simulation has been performed on (110)- RuO_2 /liquid water interface in the NVT ensemble (~ 25 ps), where the temperature was kept constant at 300 K by a Nosé-Hoover chain thermostat,^[48] adopting the Velocity-Verlet algorithm^[49] with a time step of 0.5 fs. Total spin-multiplicity default value ($=0$) has been used. Calculations/simulations have been performed with constant total number of electrons (constant charge) as in many theoretical previous studies, see e.g. Refs. [9,21,50–52].

The simulation box and its dimensions for the DFT-MD of the hydrated (110)- RuO_2 -liquid water interface are illustrated in Figure 1-a. Stoichiometric (110)- RuO_2 slab is adopted. As PBCs are applied in all 3-directions of space, when simulating the (110)- RuO_2 /water interface, a vacuum of 15.0 Å along the z-direction above the liquid (perpendicular to the surface) has

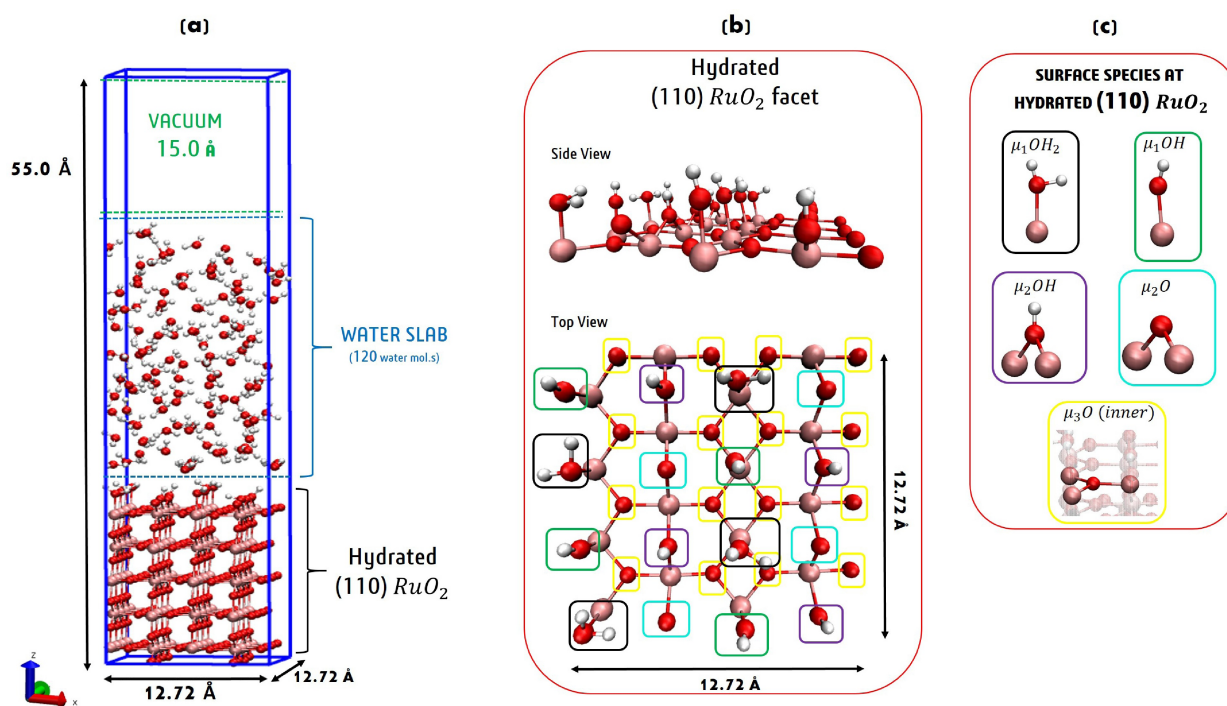


Figure 1. (a) Simulation box for the DFT-MD of the hydrated (110) RuO_2 -liquid water interface. 600 atoms: 240 solid atoms, 120 water molecules. Choice is made here to include a 15.0 Å vacuum above the liquid water in the vertical z-direction, in order not to simulate confined water due to the PBC applied in all 3-directions of space. Only one surface (the 110 upper) is put in contact with liquid water. The bottom 110 surface is in contact with vacuum. (b-c) Equilibrium composition and speciation of the (110)- RuO_2 surface in contact with liquid water. Hydrated (110)- RuO_2 surface side and top views in panel b. Ruthenium, oxygen and hydrogen atoms are colored in pink, red and white color, respectively. See text for details.

been included in the simulation box to separate the periodic z -replicas and hence avoid to simulate confined-compressed water, while keeping the simulation box dimensions reasonable and amenable to large enough time scales (for DFT-MD).

Once the (110)-RuO₂ facet is put in contact with 120 explicit water molecules (water density of ~ 1.0 g/cm³ and liquid box separately thermally equilibrated) adsorption of water molecules at the (110)-RuO₂ surface occurs, achieving the hydrated (110)-RuO₂ facet (Figure 1-b) at the oxide-water interface. In our previous work, Ref. [53], we explored water adsorption mechanisms, water organization and RuO₂ bulk model properties. In a nutshell, the rutile RuO₂ bulk has been modeled as (444) supercell (supercell approach, calculations at the Γ -point only) and the (110)-RuO₂ is composed by 5 layers-thickness in a symmetric (2 \times 4 \times 2) slab model (192 atoms), where only one surface (the 110-upper) is put in contact with water, as shown in Figure 1-a. Such a hydrated (110)-RuO₂ facet exposes therefore several surface chemical species, listed in Figure 1-c, as a result of (110) surface wettability/hydroxylation: all the surface exposed Ru atoms (8 in our model) adsorb (4 entire and 4 dissociated) water molecules keeping the surface pH (=7) neutral. Once understood the hydrated motif at the (110)-RuO₂ facet in contact with liquid water, we found that the hydrated (110)-RuO₂ can be defined as a hydrophobic surface but the (110)-RuO₂ has a strong/predominant H-bond (HB) acceptor character from the liquid water environment, *i.e.* 90% of the H-bonded surface sites are HB acceptor sites from water.^[53] See Ref. [53] for more details.

A uniform background charge and the Ewald summation for electrostatics take care of the total charge of the simulation box whenever necessary, as a standard procedure in DFT-MD simulations. In our previous work, Ref. [53], we calculated the electric field and related work function of the (110)-RuO₂ surface at the interface with vacuum and with the water slab. We found an electric field of ~ 4.8 V/Å at the (110)-RuO₂/liquid water interfacial system (same system as Figure 1-a), and a surface work function of ~ 1.8 eV, see Ref. [53] for more details. The oxidation states of atomic species involved in the here identified mechanisms of OER are calculated by employing the Maximally Localised Wannier Functions (MLWFs)^[54] analysis.

Metadynamics. Gas-phase and liquid-phase OER at (110)-RuO₂ facet have been investigated by employing enhanced sampling techniques in the DFT-MD well-tempered (WT)^[55] metadynamics^[56–58] framework as implemented in the PLUMED-2.6.2 software package,^[59] within the CP2K code.^[37,38] The free-energy profiles have been obtained by exploring the (local) configurational space (*i.e.*, the phase space) and hence probing the relevant (meta)stability basins and the connecting chemical pathway on the space spanned by a proper chosen collective variable (or reaction coordinate), that is the atomic distance between reactant atoms.

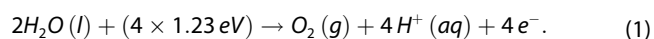
For the sake of clarity, the OER metadynamics investigation is divided in 2 reaction steps: 1) the water surface attack and dissociation step, where the distance between the oxygen O_w (of the reactant water molecule) and the O_s (oxygen of the solid surface) is chosen as unique reaction coordinate;

2) Once O_2 is achieved, the second reaction step is the $O_w = O_s$ desorption (from the RuO₂ surface), where the distance between O_s and the Ru surface atom is chosen as unique reaction coordinate. We sample each reaction step both in gas-phase and liquid-phase. More details about metadynamics sampling and how reactant O_w and O_s atoms have been chosen are given in Section 3.1.

Several WT metadynamics runs and with different starting configurations have been performed for each reaction step (see Section 3.1), in both gas and liquid phase OER, with an average simulation time of at least 30 ps for each run, checking and assuring a proper metadynamics convergence. The height (W) and the width (σ_s) of the gaussian hills added along the WT biased metadynamics are respectively 1.2 kcal/mol (initially) and 0.02 Å. Error bars estimations have been calculated performing a block analysis.^[60] Since we adopted DFT-MD metadynamics in its WT fashion,^[55] such an initial Gaussian potential height was automatically reduced (accordingly to the biasfactor γ of the WT-metadynamics set to 4) during the exploration of the configurational space as the filling procedure progressed in time, and hence a gaussian hill of decreasing W value was added every 50 fs (pace of 100 steps).

Results and Discussions

The overall process of water splitting comprises two half reactions: namely, the evolution of O₂, on the one hand, and the evolution of H₂, on the other. Such a process still represents a challenge since several issues have to be fixed in order to become economically attractive on a sizable scale. One of them is related to a significant overpotential, and therefore energy losses, at the anode surface, where oxygen in the ideal case of no-overpotential is produced via the following 4-electron-transfer OER:^[9]

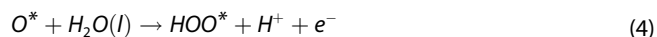


Mainly due to those high overpotential at the oxygen-evolving anode, extensive research on this subject has shown that the potential needed to split water at rates provided by the solar flux (*e.g.*, 10 mA/cm²)^[61] is limited primarily by the OER.^[62,63]

Nowadays, an important challenge is hence represented by the development and, possibly, the discovery of OER catalysts which can reduce the operative overpotential needed. Extensive research^[64] has been performed to probe valuable (photo) electrocatalysts able to lower the reaction barrier(s) and to make the OER easier to occur. As outlined in previous sections, RuO₂ has attracted a growing interest as efficient water oxidation catalyst (WOC) in the way of visible-light-driven water splitting, exhibiting a good OER activity and stability.

Modelling the OER at the (110)-RuO₂

Norskov *et al.*^[9,21] proposed, at the molecular scale, that the OER can be modelled as a complex four-steps reaction at the anode electrode as follows (the effect of liquid water was implicitly taken into account:



Gibbs free energy is usually calculated implicitly by assuming the equilibrium $H^+ + e \rightleftharpoons 1/2 H_2$ reaction at standard conditions (pH=0, pressure $p_{H_2} = 1$ bar, and T=298.15 K) and using the Gibbs free energy of hydrogen gas. In such a mechanistic decomposition, the OER reaction consists of four electrochemical steps, each of which involves one H^+/e^- transfer. The apex "*" denotes an active surface site of the catalyst and X^* a surface adsorbed X species. HO^* , O^* and HOO^* are denoted as OER intermediates, all adsorbed at the catalyst surface.

The thermodynamics free energy of the overall OER is determined by the reaction step with the highest free energy difference ΔG among the four steps shown in Eqs. (2) to (5):

$$G^{OER} = \max(\Delta G_1, \Delta G_2, \Delta G_3, \Delta G_4) \quad (6)$$

The reaction step, characterized by the highest free energy difference ΔG , is called the rate-limiting step (or potential-determining step) and it is standardly assumed to be the fundamental parameter in order to calculate the overpotential needed for the OER reaction to occur at a measurable rate. This concept was developed in previous investigations of the OER^[21,50, 51, 65] and it has been recently reviewed.^[66,67] It turned out that the catalytic performance can be estimated by the magnitude of the OER potential-determining step G^{OER} .

Overpotential generally depends on the surface reactivity of the catalyst material. In other words, surface reaction sites, surface terminations, and surface coverage profoundly affect the reaction paths leading to an increase/decrease of the required overpotential making the reaction harder/easier to occur. An open question remains about how these surface effects can affect the activity of the RuO₂ catalyst in the OER process.

When predicting the OER activity of the RuO₂ surface, several key assumptions are typically made. It is assumed that the OER occurs at a single active site following the same reaction mechanism (e.g. water nucleophilic attack) over the catalyst surface.^[68] However, there is mounting evidence suggesting a key role of the dynamic evolution of the catalyst/water interface in defining the catalytic activity, reaction mechanisms, and measured OER reaction barrier/overpotential.^[68–71]

Norskov *et al.* in a previous theoretical modeling of OER at (110) RuO₂ adopted static calculations of free-energy OER estimations, without explicit water environment and using the binding energy of the OER intermediate species HO^* and HOO^* as OER activity descriptor,^[72] estimating an OER overpotential in the 0.5–0.7 eV range. Klyukin *et al.* provided OER free energy profiles at (110) RuO₂ in contact with explicit water layers via AIMD Blue Moon ensemble approach showing that the OER overpotential can be lowered until to 0.2 eV at fully-oxidized (110) RuO₂ facet.^[68] Alexandrov *et al.*'s theoretical study investigated the OER adopting static calculations of free-energy barriers (with only one water molecule) comparing the lattice oxygen mechanism (LOM) with the conventional adsorbate evolving mechanism (AEM) of the OER at the (110) RuO₂ revealing overpotentials of around 0.38 eV and 0.79 eV for the LOM and AEM mechanism, respectively.^[73] The mentioned OER overpotential values are also listed in Table 1.

In our modeling made here, following the OER pathway as suggested in Refs. [9,21] and taking into account that oxygen evolution might be generally difficult to achieve at a single Ru–O surface site,^[68,74–77] we propose an OER pathway as our reference pathway for which reaction mechanism involves the oxidation of a water molecule via a nucleophilic water attack to the (110)-RuO₂ catalyst surface. Our reference pathway is schematically shown in Figure 2.

It proceeds through the formation of surface adsorbed intermediates HOO^* and $O = O^*$. The overall reaction can be summarized as the dissociation of a water molecule over catalytic active sites on the (110)-RuO₂ surface (step 1–2), losing one proton and forming the oxygen-oxygen bond with a surface oxygen (O_s) through the formation of the chemisorbed intermediate HOO^* (intermediate step in Figure 2). In particular, the OER proposed mechanism^[9,21] reveals step 1→2 as the oxidation of HOO^* (see intermediate step panel in Figure 2) into a $O = O^*$ surface adsorbed. Finally, the $O = O^*$ desorbs as double-bonded $O = O$ molecular oxygen (step 3), creating a surface O vacancy where a subsequent nucleophilic addition of another water molecule could spontaneously occur (step 4), and hence the OER is free to restart and continue.

Note that previous studies of water oxidation by catalysts have shown that in many cases the O-covered catalyst surface shows higher activity than the OH-covered surface, such that the OER will only occur on surfaces with a high oxygen coverage.^[68,74–77] It was also speculated, both experimentally and theoretically, that the oxygen evolution might be generally difficult to achieve at a single Ru–O surface catalyst site due to the high localization of the electronic charge. The OER should

Table 1. Comparison between OER overpotentials on (110) RuO₂ calculated by employing different theoretical models present in the literature [72], [68], [73].

OER Overpotential (ev)	Ref.
0.5–0.7	[72]
0.2	[68]
0.38 (LOM)	[73]
0.79 (AEM)	

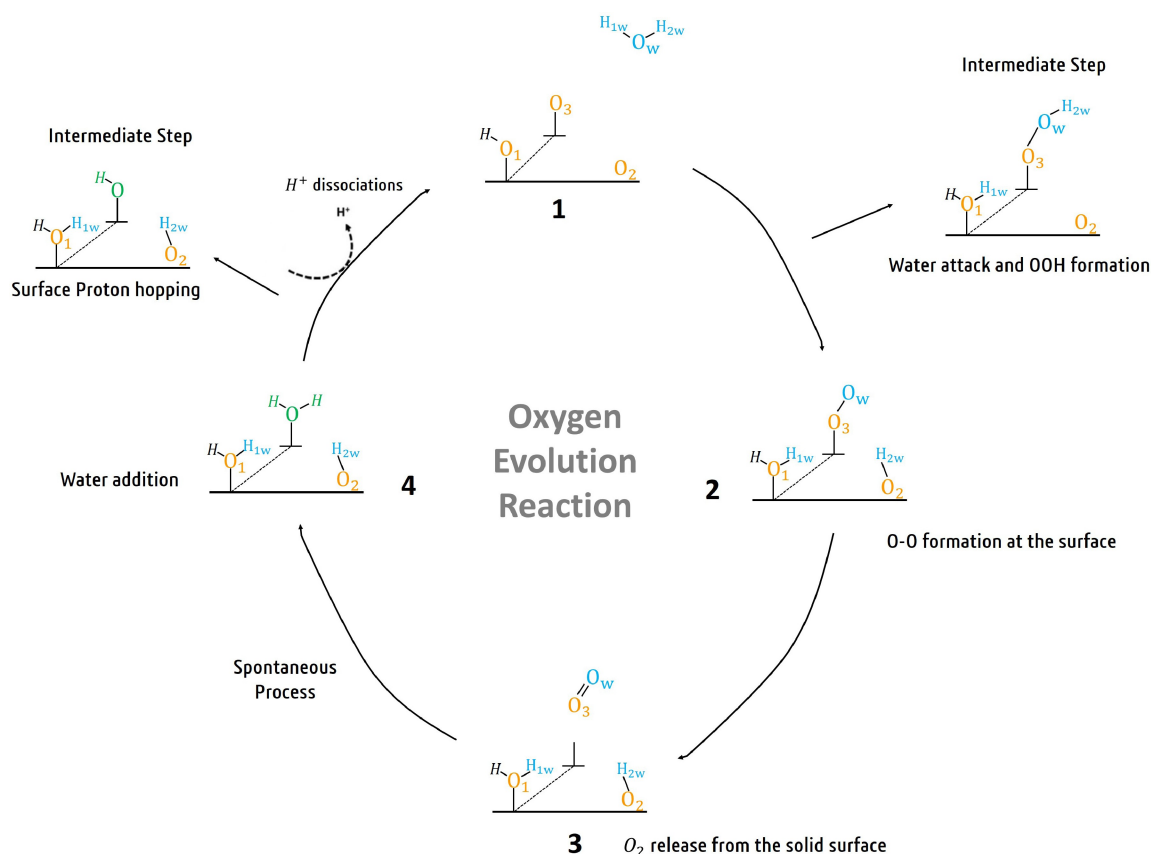


Figure 2. Proposed mechanism of the OER as our reference pathway taking place via a water attack and surface adsorbed intermediates HOO^* and $\text{O} - \text{O}^*$. Potential catalyst surface oxygens sites are in orange color. The light blue label denotes the reactant water molecule.

be easier to occur when, *at least*, two active $\text{Ru} - \text{O}$ surface sites are involved. The cooperation of these two neighbors at the WOC surface is able to make (energetically) easier the water dissociation at the catalyst surface (step 1–2 in Figure 2) and to form the desired $\text{O} - \text{O}^*$ surface adsorbed species (step 2), as provided in several theoretical and experimental studies about heterogeneous catalysts.^[68,74–77] It has been shown that lattice/termination oxygens can be involved in the OER, and the cooperation of these neighbors surface sites can lower the theoretical overpotential of OER down to 0.2 eV.^[68] A previous paper showed that a moderate overpotential of 0.64 eV is required when only a single $\text{Ru} - \text{O}$ surface catalyst site is taken into account in the oxygen evolution at the (110) RuO_2 .^[74]

If only one surface $\text{Ru} - \text{O}$ active site is available for the OER, the repulsion between the electron-rich surface O and the oxygen O of the water molecule can cause a high-energy barrier for the $\text{O} - \text{O}^*$ bond formation.^[76,77] For these highlighted reasons, and for the fact that several chemical species (see Figure 1-b) are possible OER catalyst surface sites – such as μ_1 , μ_2 and μ_3 inner sites at the hydrated (110)- RuO_2 surface pattern –, all WT metadynamics calculations (in gas and liquid phase) reported here for the OER investigations are performed with the assumption that, at least, two adjacent $\text{Ru} - \text{O}$ surface sites are available at the hydrated (110)- RuO_2 facet, as also outlined in the proposed reference OER mechanism in Figure 2.

In addition, having two adjacent available $\text{Ru} - \text{O}$ surface sites as start condition is also in agreement with experimental evidences which provide that in the OER (applied) potential region, most of the oxide surfaces (RuO_2 included) change from being HO^* -covered surface to becoming (mostly) O^* covered.^[78–84]

Note that, at the hydrated (110)- RuO_2 facet, several surface speciations are present (see Figure 1-b) and located in different surface spot that could be surface OER catalytic sites. Therefore, by selecting different surface sites and morphology scenarios as possible reactants in our metadynamics investigation, we provide a thorough evaluation of possible OER catalytic sites at the hydrated (110)- RuO_2 facet.

A schematic representation of the explored start configurations, *i.e.* of the chosen surface sites (investigated during our metadynamics runs) that could be catalytic sites for the water oxidation process, is depicted in Figure 3.

(a–c–d): one μ_1 -O, one μ_1 -OH and one μ_3 -O inner site placed in different surface locations and geometric arrangements; (b): one μ_1 -O, one μ_1 -OH and one μ_2 -O site. All the other surface sites are not modified and treated as they exist in the hydrated state at the interface with the liquid water (see Figure 1-b, c). The water molecule closest to the selected surface oxygen atoms (or surface $-\text{OH}$) colored in orange is chosen as reactant, at *time* = 0 of the biased metadynamics.

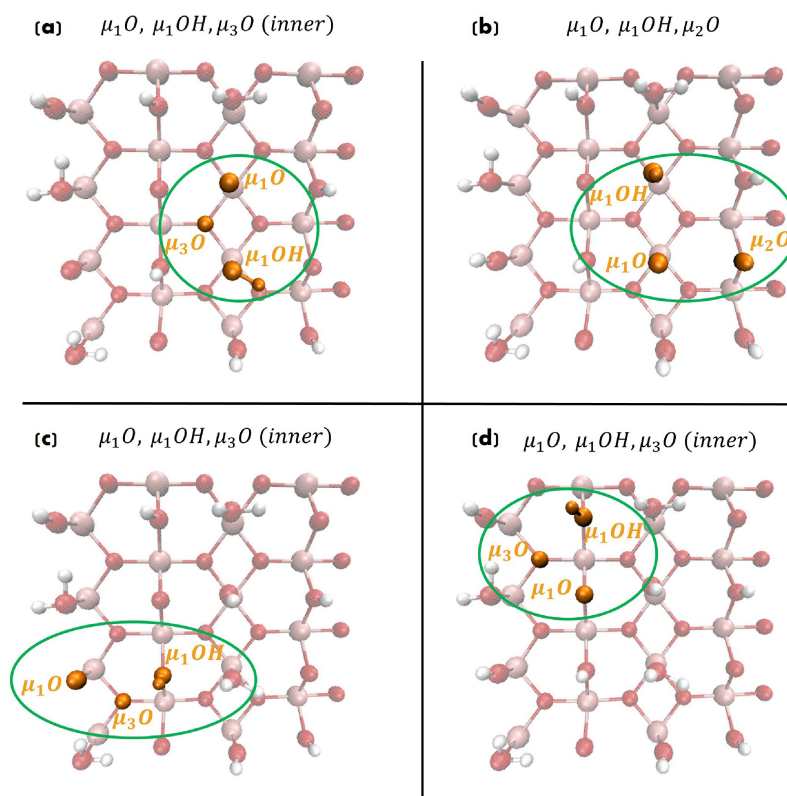


Figure 3. Top views of start configurations of the chosen surface sites as possible OER catalytic sites at the hydrated (110)-RuO₂ facet. Neighbor surface oxygen sites are displayed in orange color.

For the sake of clarity, following the OER mechanism proposed in Refs. [9,21] and taking into account the need to have (at least) two adjacent available Ru–O surface sites as start condition, in our WT metadynamics investigations the OER is schematically divided in 2 reaction steps, as follows:

1) the water attack and dissociation step, see Figure 4 step 1–2, where the distance between the oxygen O_w (of the reactant water molecule) and the O_s (surface oxygen of the solid

110-RuO₂) is chosen as unique reaction coordinate. Using the simple O_s–O_w distance as reaction coordinate is an obvious choice but may miss relevant features of the process of interest.^[23] The formation of the O–O bond together with the subsequent deprotonation of the nucleophile (water) was typically found to be the energetically most demanding reaction of the catalytic cycle and it has been proven the need of proton acceptors near the active site^[85] to facilitate the O–O

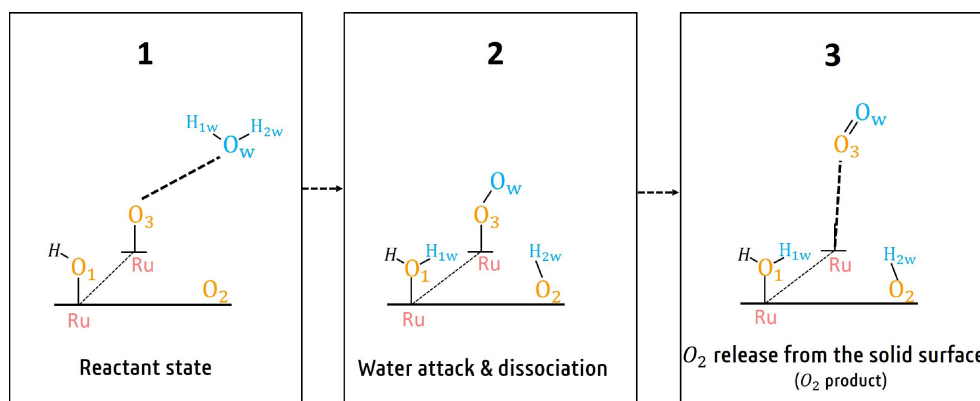


Figure 4. Modeling of the OER for our WT metadynamics investigations at the (110)-RuO₂ surface. 1–2 is the first reaction step from reactant state to (nucleophilic) water attack and water dissociation; 2–3 is the second reaction step which ends with the surface desorption of OER product, that is gas O₂. Potential catalyst surface oxygens sites are in orange color. The light blue label denotes the reactant water molecule. The dashed black lines in panel 1 and 3 denote the reaction coordinate.

bond formation. Therefore, the conjecture made here is to consider the O–O bond formation by a classical water nucleophilic attack (WNA) for which water proton-transfers can occur by the presence of catalyst proton-acceptors-sites, as outlined in the above-mentioned work.^[85] The O_3 is systematically chosen as μ_1 -O surface site.

2) $O_w = O_3$ desorption (from the 110-RuO₂ surface) step, see Figure 4 step 2–3, where the distance between O_3 and the Ru surface atom is chosen as unique reaction coordinate. The O_3 is initially bonded to Ru surface atom (see step 2 in Figure 4)

Once $O_w = O_3$ desorbs from the surface, the regeneration of surface O_3 can occur with the surface adsorption/dissociation of an additional water molecule assuring the OER restart and continue. This nucleophilic addition of another water molecule has been proved to occur spontaneously and hence is not investigated in our OER metadynamics.^[68,74–77] The OER rate-limiting step is therefore here assumed to be included in the reaction steps 1–2 and 2–3 highlighted in Figure 4.

OER activity descriptors

Activity descriptors can help in the identification and prediction of OER active oxide catalysts, and thus, they could be defined as the main catalysts' physicochemical property governing the OER activity. However, the definition of OER activity and how it is determined is at present not homogenized in the community, if even not 'chaotic'.^[70]

In 2011, Man, Rossmeisl, Norskov, *et al.*,^[9,21] showed that it is possible to identify a universal descriptor for the OER activity based on the adsorption energies of the surface adsorbed HO^* and HOO^* intermediate species on catalyst surface, *i.e.* basically looking at how weak or strong these two intermediate HO^* and HOO^* species are bound to the catalyst surface during the OER. The main parameter governing the reaction overpotential is therefore the binding strength of oxygen (or oxygenated species/intermediates) on the catalyst surface following the Sabatier principle (from which Volcano plot has been derived): the best catalyst in terms of displaying the minimum overpotential binds oxygen on its surface neither too strongly nor too weakly.^[70] According to this analysis, RuO₂ and Co₃O₄ among binary oxides and LaNiO₃ and SrCoO₃ among perovskites have the lowest theoretical overpotentials due to their optimal trade-off between strong and weak binding energy of oxygen (OER intermediates) resulting therefore at the top of Volcano plot as best OER catalysts.^[9]

This well-established understanding of the reaction mechanism and parameters driving catalyst activity has been progressively challenged over the past years by few experimental and theoretical observations pointing, among other, toward the possibility of a different reaction mechanism than the conventional one.^[70] Indeed, a rather substantial variety of activity descriptors has been proposed so far for OER catalysts, such as, for example, the number of d-electrons,^[86] the e_g -band filling of the transition-metal cations,^[87] the difference between the surface binding energies of O^* and HO^* reaction intermediates,^[9] the oxide formation energy,^[88] and the accumula-

tion of the magnetic moment,^[89] stressing out that there is currently no consensus on the activity descriptors for catalysts and hence no consensus on how to calculate (theoretical) overpotential, and least of all on the OER reaction mechanism.

Notably, as reviewed by Dau *et al.* in Ref. [66], on the surface of a real catalyst surface such as a supported metal oxide nanoparticle, the multiplicity of structurally distinct facets leads to a range of surface sites with distinctively different coordination and chemisorption properties. Generally, low-coordinated sites bind adsorbates more strongly and hence, in case of the real catalyst, there may be a small fraction of surface sites with a more favorable adsorption thermochemistry. The overall overpotential will then be a convolution of individual overpotentials of different sites. Under these conditions, it is feasible that OER is thermochemically limited by different OER steps depending on the surface site(s) of interest.^[66]

Herein, the associated free-energy surfaces have been evaluated taking the forward free-energy activation/kinetic barrier as activity descriptor, *i.e.* the amount of free-energy needed to activate/start the reaction (of the overall reaction process from reactants to the product species) for each OER step shown in Figure 4. The aim has been the identification of the OER rate limiting step. Most of the previous theoretical studies of OER catalysts mainly focused on the thermodynamic properties of the reaction intermediates without considering their free energy barriers (including transition states). However, looking at free-energy activation/kinetic barriers instead of the traditional thermodynamic free energy differences has gained enough interest and reliability to be applied for free-energy landscapes of interstellar chemical reactions^[90–92] (astrochemistry) and ultimately in electrochemistry for methanol chemistry/formaldehyde synthesis^[93] as well as for OER and overpotential calculations at the (110)-IrO₂ compound.^[29]

In this work, we focus on free energy activation barriers from metadynamics calculations in gas-phase and in explicit solvent model in contrast to traditional thermodynamic free energy differences from static calculations using implicit solvent model.^[9,21] This purely kinetic notion tacitly assumes that all elementary OER steps along the reaction pathway are not limited by thermodynamics.

OER at the hydrated (110)-RuO₂ facet: gas-phase solvent model

OER is here investigated at the (110)-RuO₂ surface in gas-phase solvent where only one water molecule is present in order to have the oxidation (OER) of the latter. Starting configurations are the same as depicted in Figure 3, where different catalytic sites are chosen in different surface arrangement, and starting water molecule position is chosen as the water molecule above (closest to) the selected catalytic sites (surface oxygen atoms or surface –OH) colored in orange, such as in Figure 5.

With the aim to fully assess the OER at the (110)-RuO₂ surface, free-energy activation/kinetic barriers are therefore estimated for each OER step shown in Figure 4.

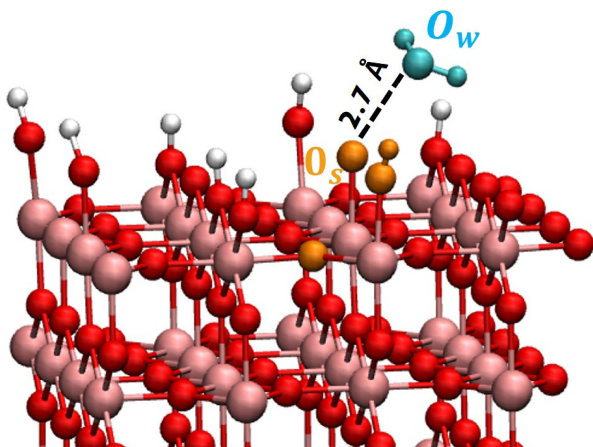


Figure 5. Side view of the hydrated (110)-RuO₂ surface in presence of only one water molecule as start configuration at *time* = 0 of the biased metadynamics. Surface sites as possible OER catalytic sites are in orange color and the reactant water molecule are in cyan color.

The first result from our WT metadynamics investigations is that, among all the explored start configurations (see Figure 3), only adjacent μ_1 -O, μ_1 -OH and μ_2 -O sites arranged as in Figure 3-a morphology scenario lead to the OER.

All the other possible OER catalytic sites placed as in in Figure 3-b-c-d (chosen as possible reactant sites) do not provide

any OER in our metadynamics simulation time for the gas-phase OER. Thus, the gas-phase OER free energy profiles by means of WT metadynamics for the reaction steps 1–2 and 2–3 highlighted in Figure 4 with start configuration as in Figure 3-a are shown in Figure 6.

The gas-phase OER starts with the water attack and its dissociation at the μ_1 -O surface site. The dissociated water hydrogen atoms hop to nearby μ_1 -OH and μ_1 -O surface sites, respectively (see panel 2 in Figure 6). A formation of an active radical group μ_1 -OOH could occur as intermediate between step 1–2. Consequently, the doubly-bonded O₂ species desorbs from the μ_1 -OO, leading to the expected O₂ gas phase formation (see panel 3 in Figure 6).

The associated free-energy surfaces (*a* and *b* panels in Figure 6) have been evaluated with the aim of determining the free-energy activation barrier of each reaction step 1–2 and 2–3 in order to identify the rate-limiting step. Thus, a free-energy activation barrier of 37.73 ± 0.5 kcal/mol (1.64 ± 0.02 eV) has to be overcome in order to start the OER by attracting and dissociating a water molecule at the hydrated (110)-RuO₂ surface (free-energy barrier in very good agreement with the one – 1.60 eV – from previous DFT study on gas-phase OER at 110-RuO₂^[21]). 10.5 ± 0.5 kcal/mol (0.46 ± 0.02 eV) are needed for the doubly-bonded O₂ desorption from the catalyst surface, confirming RuO₂ a weak binding energy of O₂.^[9]

For the sake of completeness, it is worth pointing out from our DFT MLWFs electronic analyses that O₂ (gas) product has

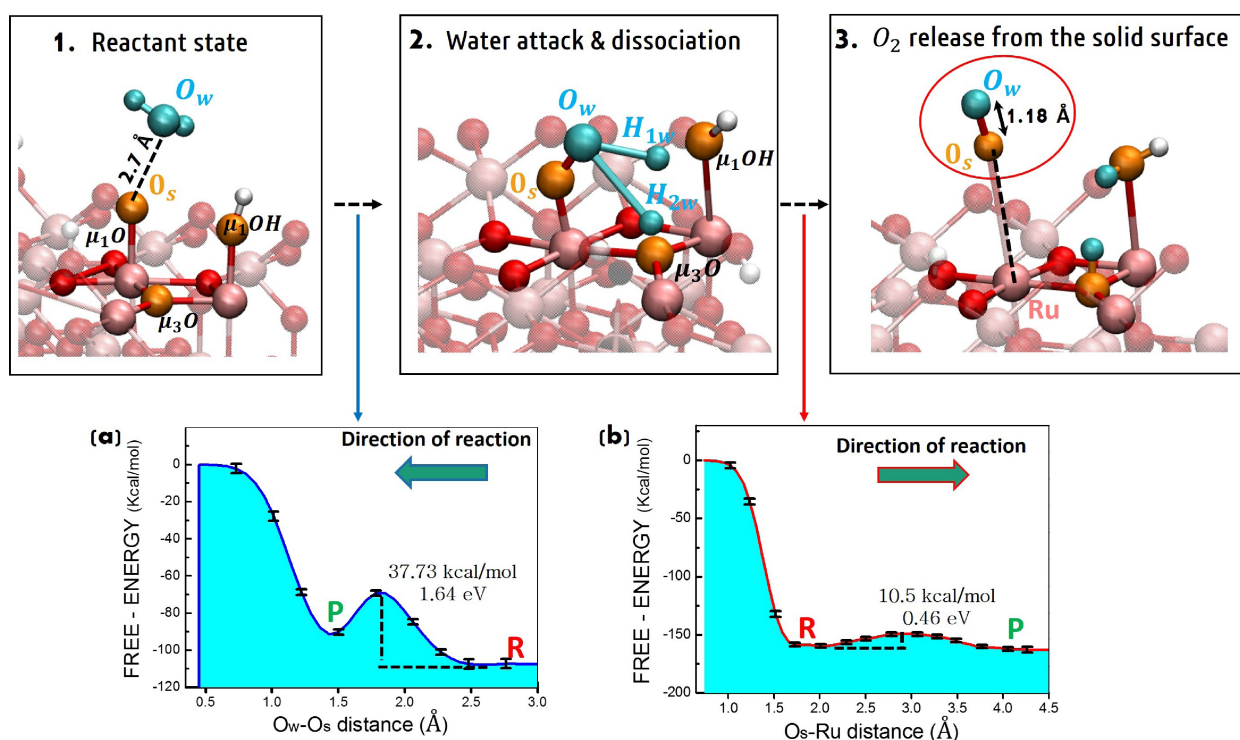


Figure 6. Snapshots from (DFT-MD) WT metadynamics simulations of successive events for the gas-phase OER at the hydrated (110)-RuO₂ surface and the associated free-energy profiles of the OER steps. Orange and light blue coloring refer to O catalyst surface sites and the (only one) reactant water molecule, respectively. The dashed black lines in panel 1 and 3 denote the reaction coordinates. Panel a and panel b are free-energy profiles of OER step 1–2 and 2–3, respectively. R and P denote the reactant and product state, respectively. The free-energy scale in the y-axis is in kcal/mol. The reaction coordinate is expressed as distance (Å) in the x-axis. The values on the free-energy profiles are the barriers expressed in kcal/mol and in eV. Error bars in black color.

been found in its electronic ground state, namely the triplet state, with two unpaired electrons in the orbital level $n = 2$ in agreement with a previous study.^[29] The same will be valid also for the O_2 obtained in our OER liquid phase investigation in the next section.

OER at the hydrated (110)- RuO_2 facet: liquid-phase solvent model

We now investigate the OER at the hydrated (110)- RuO_2 /liquid water interface where a water slab (120 water molecules, density $\sim 1.0 \text{ g/cm}^3$) is explicitly considered (see Figure 1-a), overcoming the aforementioned limit of the current literature in adopting only, at the best, one water molecule or a water monolayer in contact with the catalyst surface. This way, the condensed-phase OER and the hydrated (110)- RuO_2 as catalyst can be more accurately characterized. As already done for the OER gas-phase model at the hydrated (110)- RuO_2 in the previous section, the free-energy activation barrier (hence the associated activation overpotential as well) are therefore estimated for each OER step of the adopted metadynamics setup shown in Figure 4. For the purpose of comparison, the reactant water molecule in our OER liquid-phase is chosen as the same reactant water molecule in gas-phase.

As partly expected, we will see in the following that the presence of the interfacial aqueous environment now leads to more possibilities for the reactivity, and two possible reaction

pathways for the OER at the hydrated (110)- RuO_2 in contact with water will be identified.

The first OER pathway, shown in Figure 7, is similar to the one identified in gas-phase:

Active OER catalyst sites are here identified in adjacent μ_1 -O, μ_1 -OH and μ_2 -O sites at the surface arranged as in the morphology scenario shown in Figure 3-b.

A free-energy activation barrier of $34.8 \pm 0.7 \text{ kcal/mol}$ ($1.51 \pm 0.03 \text{ eV}$) has to be overcome in order to start the OER attracting and dissociating a water molecule (from the water environment) at the μ_1 -O surface site, and $10.8 \pm 0.5 \text{ kcal/mol}$ ($0.47 \pm 0.02 \text{ eV}$) are needed for the doubly-bonded O_2 desorption from the catalyst surface, this latter being very similar to the free-energy barrier of 10.5 kcal/mol (0.46 eV) found in gas-phase OER (in the previous section) for the O_2 desorption.

The dissociated water hydrogen atoms hop to a nearby μ_1 -OH and μ_2 -O surface sites, respectively (see panel 2 in Figure 7) and a formation of an active radical group μ_1 -OOH occurs as intermediate between steps 1–2, as already seen for the gas-phase OER.

The OER rate-limiting step is also here the water attack and dissociation step at the μ_1 -O surface site, as shown in step 1–2 in Figure 7. However, contrarily to the gas-phase counterpart, reactants and products are found separated by a lower free-energy barrier of about 34.8 kcal/mol (1.51 eV).

Therefore, from this first identified OER liquid-phase pathway, it appears that the presence of an explicit aqueous environment and accordingly the kinetics of the water environment somehow enhance the surface activity at the hydrated

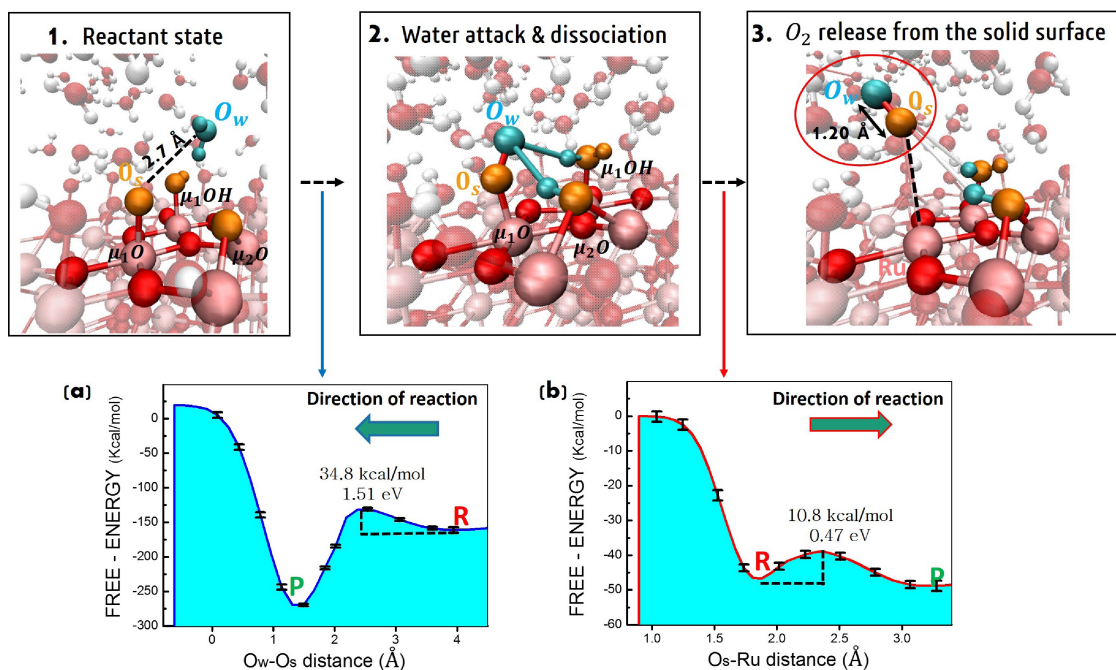


Figure 7. Path 1: snapshots from (DFT-MD) WT metadynamics simulations of successive events for the liquid-phase OER at the hydrated (110)- RuO_2 surface and the associated free-energy profiles of the OER steps. Orange and light blue coloring refer to O catalyst surface sites and the reactant water molecule, respectively. The dashed black lines in panel 1 and 3 denote the reaction coordinates. Panel a and panel b are free-energy profiles of OER step 1–2 and 2–3, respectively. R and P denote the reactant and product state, respectively. The free-energy scale in the y-axis is in kcal/mol. The reaction coordinate is expressed as distance (\AA) in the x-axis. The values on the free-energy profiles are the barriers expressed in kcal/mol and in eV. Error bars in black color.

(110)-RuO₂ facet and hence a lower free-energy barrier is required for the O₂ evolution in comparison with the previously identified gas-phase OER pathway.

OER Water-Assisted Pathway. On the other hand, our WT metadynamics simulations at the hydrated (110)-RuO₂/water interface show an alternative OER reaction route which, surprisingly, has a noticeable lower free-energy barrier. The here found alternative OER liquid-phase results for reaction steps 1–2 and 2–3 are shown in Figure 8.

A free-energy activation barrier of 20.5 ± 0.5 kcal/mol (0.89 ± 0.02 eV) has to be overcome in order to start the OER attracting and dissociating a water molecule (from the water environment) at the hydrated (110)-RuO₂ surface, and 10.2 ± 0.5 kcal/mol (0.44 ± 0.02 eV) are needed for the double-bonded O₂ desorption from the catalyst surface, this latter being very similar to the free-energy barrier of 10.5 kcal/mol (0.46 eV) found in gas-phase OER and the mechanism discussed in the previous section for the O₂ desorption.

As already seen for the previous OER pathways, the liquid phase OER rate-limiting step is also here identified by the water attack and dissociation step at the μ_1 -O surface site, as shown in step 1–2 in Figure 8. However, contrarily to our previous gas-phase and liquid phase OER investigations, we now obtain a free-energy barrier of 20.5 kcal/mol (0.89 eV) that is almost half-value of the free-energy barrier obtained in gas-phase (37.73 kcal/mol = 1.64 eV) and still lower than the free-energy barrier obtained in the previous liquid phase reaction (path-1) pathway (34.8 kcal/mol = 1.51 eV).

This is due to the fact that the reaction now proceeds preferentially through a water-assisted one-step mechanism with a proton transfer from the reactant water molecule to a neighboring one (see Figure 8 panel 2). More specifically, the reaction starts with the water dissociation above the μ_1 -O catalyst surface site (as already seen for the gas-phase OER). However, contrarily to previous OER routes, only one dissociated hydrogen H_{1w} of the water molecule is surface adsorbed, at the μ_2 -O site. The other dissociated water hydrogen H_{2w} energetically and kinetically prefers to hop toward a nearby water molecule of the surrounding water environment, as depicted in the panel 2 of Figure 8. The final step of this concerted reaction is represented, as expected, by the O₂ desorption shown in the panel 3 of Figure 8. The surface catalyst sites are not anymore 3 adjacent surface sites (as detected for previous OER pathways) but just adjacent μ_1 -O and μ_1 -OH (and a water molecule from the water environment) are enough in catalyzing the OER, as outlined in Figure 8–2.

In the here found liquid phase OER pathway, the water molecule does not act as a ‘spectator’ but it plays a crucial role in the kinetic evolution of the OER and hence enhancing it. It is worth to remark that such a water-assisted OER mechanism is different from the OER pathways proposed by Norskov *et al.*^[9,21] and most of the OER studies in the literature (for surfaces) which suffer from the lack of an explicit solvent model, and for which the dissociated hydrogen atoms of the water molecule are therefore systematically surface adsorbed (as in our gas-phase scenario in Figure 6). Due to the key role of the water environment as co-reactant found here, the condensed phase

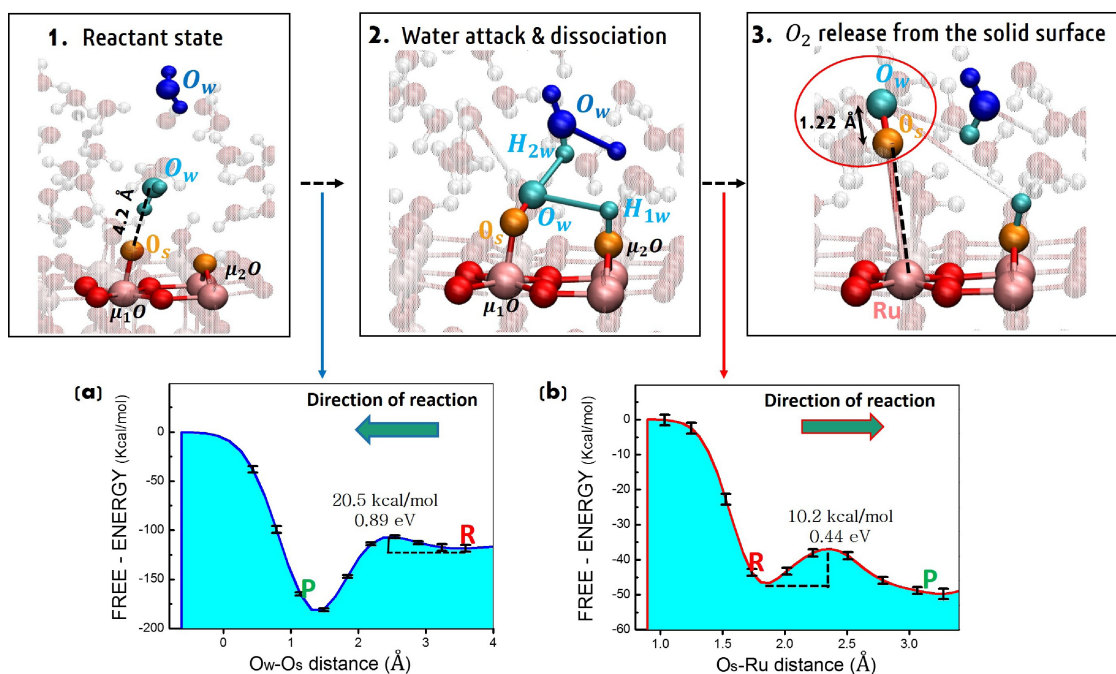


Figure 8. Path 2: snapshots from (DFT-MD) WT metadynamics simulations of successive events for the liquid-phase OER at the hydrated (110)-RuO₂ surface and the associated free-energy profiles of the OER steps. Orange and light blue coloring refer to O catalyst surface sites and the reactant water molecule, respectively. The dashed black lines in panel 1 and 3 denote the reaction coordinates. Panel a and panel b are free-energy profiles of OER step 1–2 and 2–3, respectively. R and P denote the reactant and product state, respectively. The free-energy scale in the y-axis is in kcal/mol. The reaction coordinate is expressed as distance (Å) in the x-axis. The values on the free-energy profiles are the barriers expressed in kcal/mol and in eV. Error bars in black color.

OER scenario (Figure 8) turns out to have an unprecedented free energy barrier smaller than the gas-phase counterpart.

For the sake of completeness, our DFT MLWFs electronic analyses suggest that the OER catalytic site μ_1 -O has been found as $\text{Ru}^{\text{VI}}\text{-O}$, in agreement with previous experimental and theoretical evidences.^[68,94–96] As outlined in our previous work (Ref. [53]), note that the water addition on the Ru^{IV} surface site can occur also as dissociated water molecule (surface adsorbed) leading to the formation of -OH surface adsorbed instead of -OH_2 .

In a nutshell, the catalytic action of the water environment at the interface plays a key role in lowering the OER free-energy barrier. This result is somehow expected and conform to the evidence that condensed-phase reactions are, in general, less demanding in terms of free energy,^[97–99] considering also the different weight of the entropic contributions in between gas- and condensed-phase processes.

Conclusions

A study the OER for (110)- RuO_2 /water interface is presented not only by looking at the catalyst, but also by addressing the role of an explicit water environment in the catalytic process of interest. To this end, spin-polarized DFT-MD coupled with state-of-the-art WT metadynamics has been applied for a global understanding of (110)- RuO_2 aqueous interface in catalyzing the O_2 evolution. This work provides the reference knowledge in the interfacial electronic, structural, dynamical properties at this promising interface for water oxidation.

We have shown how important it is to take into consideration the presence of the water environment in the structural characterization of catalyst surface. The wettability of the (110)- RuO_2 surface plays a key role in the chemical activity of the surface, enhancing therefore its ability to catalyze the O_2 evolution. Moreover, the fine characterization of (110)- RuO_2 presented here would not have been achievable if only one water molecule/layer or implicit solvent model would have been adopted such as in most studies in literature.

The present study provides an innovative state-of-the-art theoretical/computational strategy for the investigation of the OER, and identifies possible catalyst sites without ambiguity. In this context, by investigating the OER on the (110)- RuO_2 surface, our DFT WT metadynamics provides that active OER catalyst sites are identified in adjacent μ_1 -O, μ_1 -OH and μ_3 -O inner sites (Figure 3-a) at the surface in gas-phase and in μ_1 -O and μ_1 -OH sites (Figure 3-b) for the energetically favored path in liquid phase OER. We also reveal that the (nucleophilic) water attack and dissociation occurs systematically at the μ_1 -O surface sites in $\text{Ru}^{\text{VI}}\text{-O}$ oxidation state.

Moreover, it is clear that not only the formation of surface oxygen bond (between O_2 product) holds a key role in shaping the free-energy surface of the OER, but also the topological arrangement of the catalyst sites at the surface has a prominent contribution in determining the free-energy barrier height. Accordingly, only the geometrical spatial arrangements as depicted in Figure 3-a, b are able to catalyze the OER at (110)-

RuO_2 . This is due to the fact that such arrangements, thanks to the closeness of the sites (*i.e.* these surface catalyst sites are only ~ 2.6 Å apart from each others), are able to provide a restricted catalytic spot at the surface area enhancing therefore the OER to occur. The existence of a specific distance between surface sites on a given surface conferring to the latter efficient catalytic properties has also recently been demonstrated at silica surfaces.^[100]

Interestingly, comparing gas-phase and liquid-phase OER FESs, an unprecedented OER pathway with low free energy barrier is found in the liquid phase. Such a novel free-energy pathway identified at the (110)- RuO_2 liquid water interface differs from the OER pathways proposed in the literature for which hydrogens of the dissociated water molecule are systematically surface adsorbed due to the lack of an explicit water environment. Water molecules here thus do not act as a 'guest' but they are explicitly involved in the lowest free-energy OER mechanism identified: in particular, one dissociated water hydrogen hops toward a neighbor water molecule of the surrounding water environment.

We have identified, for the first time, that water acts as OER co-reactant and co-catalyst (for surface catalyst), and hence this coupled water behaviour is crucial in lowering the OER free-energy barrier. This suggests that the synergistic effect between surface catalyst and explicit water environment dynamics is an important and not-negligible basis for a rational design of novel catalysts based on non-precious materials in the context of sunlight-driven artificial photosynthesis.

Furthermore, our results clearly demonstrate the relevance of *ab initio* molecular dynamics simulations in combination with the here adopted metadynamics technique in the rationalization of several interfacial properties and in the comprehension of reactions occurring at solid/water interfaces, also showing the importance of the presence of an explicit water environment and its interfacial reaction dynamics in modeling the OER. Similar modelling can be applied to other facets of the rutile RuO_2 – or other materials relevant for the design of efficient and sustainable heterogeneous catalysts – in contact with liquid water or other solvents, potentially relevant for the OER. The same methodology can also be applied when supported electrolytes would be present at the interface, which would be required in order to model more relevant (photo) electrochemical conditions. The finding of a novel – highly efficient – reaction route for the OER strongly also points out the urgency for its experimental characterization.

Acknowledgments

This work is embedded as part of the 'LightChEC - Solar Light to Chemical Energy Conversion' research priority program. The work was supported by the University of Zurich and the Swiss National Science Foundation (Grant No. PP00P2170667). The authors thank the Swiss National Super-computing Center for Computing Resources (Project IDs: s875 and s1001) and Prace project 119. Open access funding provided by Universitat Zurich.

Conflict of Interest

The authors declare no conflict of interest.

Keywords: Water-Assisted Chemical Route Towards the Oxygen Evolution Reaction at the Hydrated (110) Ruthenium Oxide Surface: Heterogeneous Catalysis via DFT-MD and Metadynamics

- [1] R. E. Blankenship, D. M. Tiede, J. Barber, G. W. Brudvig, G. Fleming, M. Ghirardi, M. Gunner, W. Junge, D. M. Kramer, A. Melis, *Science* **2011**, *332*, 805.
- [2] Y. Tachibana, L. Vayssieres, J. R. Durrant, *Nat. Photonics* **2012**, *6*, 511.
- [3] N. S. Lewis, D. G. Nocera, *Proc. Natl. Acad. Sci. USA* **2006**, *103*, 15729.
- [4] J. D. Blakemore, R. H. Crabtree, G. W. Brudvig, *Chem. Rev.* **2015**, *115*, 12974.
- [5] L. Francàs, R. Bofill, J. García-Antón, L. Escriche, X. Sala, A. Llobet, *Mol. Catal.* **2014**, *29*.
- [6] G. J. Kavarnos, N. J. Turro, *Chem. Rev.* **1986**, *86*, 401.
- [7] H. Over, *Chem. Rev.* **2012**, *112*, 3356.
- [8] T. Reier, M. Oezaslan, P. Strasser, *ACS Catal.* **2012**, *2*, 1765.
- [9] I. C. Man, H.-Y. Su, F. Calle-Vallejo, H. A. Hansen, J. I. Martínez, N. G. Inoglu, J. Kitchin, T. F. Jaramillo, J. K. Nørskov, J. Rossmeisl, *ChemCatChem* **2011**, *3*, 1159.
- [10] J. Park, J. W. Lee, B. U. Ye, S. H. Chun, S. H. Joo, H. Park, H. Lee, H. Y. Jeong, M. H. Kim, J. M. Baik, *Sci. Rep.* **2015**, *5*, 1.
- [11] S. D. Tilley, M. Schreier, J. Azevedo, M. Stefik, M. Graetzel, *Adv. Funct. Mater.* **2014**, *24*, 303.
- [12] J. Lee, S. A. S. Shah, P. J. Yoo, B. Lim, *Chem. Phys. Lett.* **2017**, *673*, 89.
- [13] Y. D. Kim, S. Schwegmann, A. P. Seitsonen, H. Over, *J. Phys. Chem. B* **2001**, *105*, 2205.
- [14] H. Over, Y. D. Kim, A. Seitsonen, S. Wendt, E. Lundgren, M. Schmid, P. Varga, A. Morgante, G. Ertl, *Science* **2000**, *287*, 1474.
- [15] A. Lobo, H. Conrad, *Surf. Sci.* **2003**, *523*, 279.
- [16] Y.-H. Fang, Z.-P. Liu, *J. Am. Chem. Soc.* **2010**, *132*, 18214.
- [17] T. Wang, J. Jelic, D. Rosenthal, K. Reuter, arXiv preprint arXiv:1303.4203 2013.
- [18] A. Stirling, N. N. Nair, A. Lledós, G. Ujaque, *Chem. Soc. Rev.* **2014**, *43*, 4940.
- [19] A. Bouzid, A. Pasquarello, *J. Phys. Chem. Lett.* **2018**, *9*, 1880.
- [20] V. Stamenkovic, B. S. Mun, K. J. Mayrhofer, P. N. Ross, N. M. Markovic, J. Rossmeisl, J. Greeley, J. K. Nørskov, *Angew. Chem.* **2006**, *118*, 2963.
- [21] J. Rossmeisl, Z.-W. Qu, H. Zhu, G.-J. Kroes, J. K. Nørskov, *J. Electroanal. Chem.* **2007**, *607*, 83.
- [22] M. Schilling, R. A. Cunha, S. Lubner, *ACS Catal.* **2020**, *10*, 7657.
- [23] M. Schilling, R. A. Cunha, S. Lubner, *J. Chem. Theory Comput.* **2020**, *16*, 2436.
- [24] D. Scherrer, M. Schilling, S. Lubner, T. Fox, B. Spingler, R. Alberto, C. J. Richmond, *Dalton Trans.* **2016**, *45*, 19361.
- [25] M. Gil-Sepulcre, M. Schilling, M. Boehler, F. Bozoglian, C. Bachmann, D. Scherrer, T. Fox, B. Spingler, C. Gimbert-Surinach, R. Alberto, *ChemSusChem* **2017**.
- [26] L. Duan, F. Bozoglian, S. Mandal, B. Stewart, T. Privalov, A. Llobet, L. Sun, *Nat. Chem.* **2012**, *4*, 418.
- [27] L. Tong, L. Duan, Y. Xu, T. Privalov, L. Sun, *Angew. Chem. Int. Ed.* **2011**, *50*, 445.
- [28] E. Watanabe, J. Rossmeisl, M. E. Bjorketun, H. Ushiyama, K. Yamashita, *J. Phys. Chem. C* **2016**, *120*, 8096.
- [29] Y. Ping, R. J. Nielsen, W. A. Goddard III, *J. Am. Chem. Soc.* **2017**, *139*, 149.
- [30] A. Zagalskaya, I. Evazzade, V. Alexandrov, *ACS Energy Lett.* **2021**, *6*, 1124.
- [31] F. Creazzo, S. Pezzotti, S. Bougueroua, A. Serva, J. Sponer, F. Saija, G. Cassone, M.-P. Gaigeot, *Phys. Chem. Chem. Phys.* **2020**, *22*, 10438.
- [32] G. Cassone, F. Creazzo, P. V. Giaquinta, F. Saija, A. M. Saitta, *Phys. Chem. Chem. Phys.* **2016**, *18*, 23164.
- [33] G. Cassone, F. Creazzo, P. V. Giaquinta, J. Sponer, F. Saija, *Phys. Chem. Chem. Phys.* **2017**, *19*, 20420.
- [34] G. Cassone, F. Creazzo, F. Saija, *Mol. Simul.* **2019**, *45*, 373.
- [35] A. M. Saitta, F. Saija, P. V. Giaquinta, *Phys. Rev. Lett.* **2012**, *108*, 207801.
- [36] G. Cassone, *J. Phys. Chem. Lett.* **2020**, *11*, 8983.
- [37] J. Hutter, M. Iannuzzi, F. Schiffmann, J. VandeVondele, *WIREs Comput. Mol. Sci.* **2014**, *4*, 15.
- [38] J. VandeVondele, M. Krack, F. Mohamed, M. Parrinello, T. Chassaing, J. Hutter, *Comp. Phys. Commun.* **2005**, *167*, 103.
- [39] K. Burke, J. Perdew, M. Ernzerhof, *Phys. Rev. Lett.* **1997**, *78*, 1396.
- [40] J. De Almeida, R. Ahuja, *Phys. Rev. B* **2006**, *73*, 165102.
- [41] N. Mehtougui, D. Rached, R. Khenata, H. Rached, M. Rabah, S. Bin-Omran, *Mater. Sci. Semicond. Process.* **2012**, *15*, 331.
- [42] S. Schnur, A. Groß, *New J. Phys.* **2009**, *11*, 125003.
- [43] J. A. White, E. Schwegler, G. Galli, F. Gygi, *J. Chem. Phys.* **2000**, *113*, 4668.
- [44] S. Goedecker, M. Teter, J. Hutter, *Phys. Rev. B* **1996**, *54*, 1703.
- [45] J. VandeVondele, J. Hutter, *J. Chem. Phys.* **2007**, *127*, 114105.
- [46] S. Grimme, *J. Comput. Chem.* **2004**, *25*, 1463.
- [47] S. Grimme, *J. Comput. Chem.* **2006**, *27*, 1787.
- [48] D. J. Evans, B. L. Holian, *J. Chem. Phys.* **1985**, *83*, 4069.
- [49] L. Verlet, *Phys. Rev.* **1967**, *159*, 98.
- [50] J. K. Nørskov, J. Rossmeisl, A. Logadottir, L. Lindqvist, J. R. Kitchin, T. Bligaard, H. Jonsson, *J. Phys. Chem. B* **2004**, *108*, 17886.
- [51] J. Rossmeisl, A. Logadottir, J. K. Nørskov, *Chem. Phys.* **2005**, *319*, 178.
- [52] J. K. Nørskov, T. Bligaard, J. Rossmeisl, C. H. Christensen, *Nat. Chem.* **2009**, *1*, 37.
- [53] F. Creazzo, S. Lubner, *Applied Surface Science*, Accepted.
- [54] N. Marzari, A. A. Mostofi, J. R. Yates, I. Souza, D. Vanderbilt, *Rev. Mod. Phys.* **2012**, *84*, 1419.
- [55] A. Barducci, G. Bussi, M. Parrinello, *Phys. Rev. Lett.* **2008**, *100*, 020603.
- [56] D. Branduardi, F. L. Gervasio, M. Parrinello, *J. Chem. Phys.* **2007**, *126*, 054103.
- [57] B. Ensing, M. De Vivo, Z. Liu, P. Moore, M. L. Klein, *Acc. Chem. Res.* **2006**, *39*, 73.
- [58] A. Laio, M. Parrinello, *Proc. Natl. Acad. Sci. USA* **2002**, *99*, 12562.
- [59] G. A. Tribello, M. Bonomi, D. Branduardi, C. Camilloni, G. Bussi, *Comput. Phys. Commun.* **2014**, *185*, 604.
- [60] H. Flyvbjerg, H. G. Petersen, *J. Chem. Phys.* **1989**, *91*, 461.
- [61] C. C. McCrory, S. Jung, J. C. Peters, T. F. Jaramillo, *J. Am. Chem. Soc.* **2013**, *135*, 16977.
- [62] M. G. Walter, E. L. Warren, J. R. McKone, S. W. Boettcher, Q. Mi, E. A. Santori, N. S. Lewis, *Chem. Rev.* **2010**, *110*, 6446.
- [63] T. R. Cook, D. K. Dogutan, S. Y. Reece, Y. Surendranath, T. S. Teets, D. G. Nocera, *Chem. Rev.* **2010**, *110*, 6474.
- [64] M. S. Burke, L. J. Enman, A. S. Batchellor, S. Zou, S. W. Boettcher, *Chem. Mater.* **2015**, *27*, 7549.
- [65] A. Valdes, Z.-W. Qu, G.-J. Kroes, J. Rossmeisl, J. K. Nørskov, *J. Phys. Chem. C* **2008**, *112*, 9872.
- [66] H. Dau, C. Limberg, T. Reier, M. Risch, S. Roggan, P. Strasser, *ChemCatChem* **2010**, *2*, 724.
- [67] H. A. Hansen, J. Rossmeisl, J. K. Nørskov, *Phys. Chem. Chem. Phys.* **2008**, *10*, 3722.
- [68] K. Klyukin, A. Zagalskaya, V. Alexandrov, *J. Phys. Chem. C* **2019**, *123*, 22151.
- [69] A. Grimaud, O. Diaz-Morales, B. Han, W. T. Hong, Y.-L. Lee, L. Giordano, K. A. Stoerzinger, M. T. Koper, Y. Shao-Horn, *Nat. Chem.* **2017**, *9*, 457.
- [70] E. Fabbri, T. J. Schmidt, *ACS Publications* **2018**, *8*, 9765–9774.
- [71] S. Geiger, O. Kasian, M. Ledendecker, E. Pizzutillo, A. M. Mingos, W. T. Fu, O. Diaz-Morales, Z. Li, T. Oellers, L. Fruchter, *Nature Catalysis* **2018**, *1*, 508.
- [72] C. F. Dickens, J. K. Nørskov, *J. Phys. Chem. C* **2017**, *121*, 18516.
- [73] A. Zagalskaya, V. Alexandrov, *ACS Catal.* **2020**, *10*, 3650.
- [74] J. Wirth, S. Monturet, T. Klamroth, P. Saalfrank, *EPL* **2011**, *93*, 68001.
- [75] J. Yu, Q. He, G. Yang, W. Zhou, Z. Shao, M. Ni, *ACS Catal.* **2019**, *9*, 9973.
- [76] C. P. Plaisance, R. A. van Santen, *J. Am. Chem. Soc.* **2015**, *137*, 14660.
- [77] H. H. Pham, M.-J. Cheng, H. Frei, L.-W. Wang, *ACS Catal.* **2016**, *6*, 5610.
- [78] B. S. Yeo, A. T. Bell, *J. Am. Chem. Soc.* **2011**, *133*, 5587.
- [79] A. Bergmann, E. Martinez-Moreno, D. Teschner, P. Cherev, M. Gliach, J. F. De Araujo, T. Reier, H. Dau, P. Strasser, *Nat. Commun.* **2015**, *6*, 1.
- [80] Z. L. Zhao, Q. Wang, X. Huang, Q. Feng, S. Gu, Z. Zhang, H. Xu, L. Zeng, M. Gu, H. Li, *Energy Environ. Sci.* **2020**, *13*, 5143.
- [81] Y. Lin, Z. Tian, L. Zhang, J. Ma, Z. Jiang, B. J. Deibert, R. Ge, L. Chen, *Nat. Commun.* **2019**, *10*, 1.
- [82] S. Laha, Y. Lee, F. Podjaski, D. Weber, V. Duppel, L. M. Schoop, F. Pielnhofer, C. Scheurer, K. Müller, U. Starke, *Adv. Eng. Mater.* **2019**, *9*, 1803795.
- [83] Y. Matsumoto, E. Sato, *Mater. Chem. Phys.* **1986**, *14*, 397.
- [84] F. Reikowski, F. Maroun, I. Pacheco, T. Wiegmann, P. Allongue, J. Stettner, O. M. Magnussen, *ACS Catal.* **2019**, *9*, 3811.

- [85] Y. Shao, H. J. de Groot, F. Buda, *J. Phys. Chem. Lett.* **2019**, *10*, 7690.
[86] J. O. Bockris, T. Otagawa, *J. Electrochem. Soc.* **1984**, *131*, 290.
[87] J. Suntivich, K. J. May, H. A. Gasteiger, J. B. Goodenough, Y. Shao-Horn, *Science* **2011**, *334*, 1383.
[88] F. Calle-Vallejo, O. A. Díaz-Morales, M. J. Kolb, M. T. Koper, *ACS Catal.* **2015**, *5*, 869.
[89] T. Lim, J. Niemantsverdriet, J. Gracia, *ChemCatChem* **2016**, *8*, 2968.
[90] G. Cassone, F. Saija, J. Sponer, J. E. Sponer, A. Jiménez-Escobar, A. Ciaravella, C. Cecchi-Pestellini, *Mon. Not. R. Astron. Soc.* **2021**, *504*, 1565.
[91] G. Cassone, J. Sponer, J. E. Sponer, F. Pietrucci, A. M. Saitta, F. Saija, *Chem. Commun.* **2018**, *54*, 3211.
[92] M. Ferus, F. Pietrucci, A. Saitta, O. Ivanek, A. Knizek, P. Kubelík, M. Krus, L. Juha, R. Dudzak, J. Dostál, *Astron. Astrophys.* **2019**, *626*, A52.
[93] G. Cassone, F. Pietrucci, F. Saija, F. Guyot, A. M. Saitta, *Chem. Sci.* **2017**, *8*, 2329.
[94] R. Kötz, H. Lewerenz, S. Stucki, *J. Electrochem. Soc.* **1983**, *130*, 825.
[95] M. E. Lyons, S. Floquet, *Phys. Chem. Chem. Phys.* **2011**, *13*, 5314.
[96] R. L. Doyle, I. J. Godwin, M. P. Brandon, M. E. Lyons, *Phys. Chem. Chem. Phys.* **2013**, *15*, 13737.
[97] F. F. Crim, *Faraday Discuss.* **2012**, *157*, 9.
[98] A. J. Orr-Ewing, D. R. Glowacki, S. J. Greaves, R. A. Rose, *J. Phys. Chem. Lett.* **2011**, *2*, 1139.
[99] A. J. Orr-Ewing, *J. Chem. Phys.* **2014**, *140*, 090901.
[100] A. Rimola, M. Fabbiani, M. Sodupe, P. Ugliengo, G. Martra, *ACS Catal.* **2018**, *8*, 4558.

Manuscript received: June 30, 2021

Accepted manuscript online: September 6, 2021

Version of record online: October 15, 2021